First-principles study of possible shallow donors in $ZnAl_2O_4$ spinel

H. Dixit
CMT-group, Departement Fysica, Universiteit Antwerpen, Groenenborgerlaan 171, B-2020 Antwerpen, Belgium

Nandan Tandon*
Instituut voor Kern- en Stralingsfysica, K. U. Leuven, Celestijnenlaan 200D, B-3001 Leuven, Belgium

S. Cottenier
Center for Molecular Modeling and Department of Materials Science and Engineering, Ghent University, Technologiepark 903, B-9052 Zwijnaarde, Belgium

R. Saniz, D. Lamoen, and B. Partoens
CMT-group and EMAT, Departement Fysica, Universiteit Antwerpen, Groenenborgerlaan 171, B-2020 Antwerpen, Belgium
(Received 30 October 2012; revised manuscript received 19 March 2013; published 7 May 2013)

$ZnAl_2O_4$ (gahnite) is a ceramic which is considered a possible transparent conducting oxide (TCO) due to its wide band gap and transparency for UV. Defects play an important role in controlling the conductivity of a TCO material along with the dopant, which is the main source of conductivity in an otherwise insulating oxide. A comprehensive first-principles density functional theory study for point defects in $ZnAl_2O_4$ spinel is presented using the Heyd, Scuseria, and Ernzerhof hybrid functional (HSE06) to overcome the band gap problem. We have investigated the formation energies of intrinsic defects which include the Zn, Al, and O vacancy and the antisite defects: Zn at the Al site (Zn_{Al}) and Al at the Zn site (Al_{Zn}). The antisite defect Al_{Zn} has the lowest formation energy and acts as a shallow donor, indicating possible *n*-type conductivity in $ZnAl_2O_4$ spinel by Al doping.

DOI: 10.1103/PhysRevB.87.174101 PACS number(s): 71.10.−w, 71.15.−m, 71.20.Nr

I. INTRODUCTION

Transparent conducting oxides (TCOs) represent a technologically important class of materials and are utilized as electrodes in many commercial applications such as flat panel displays,[1] organic light-emitting diodes,[2] and photovoltaic cell,[3] to name a few. The most commonly used TCO is indium oxide doped with tin (ITO); however, the limited availability of indium makes it an expensive material. Hence one important aspect of TCO research is to find cheaper alternatives to ITO while maintaining its high conductivity and transparency over the visible spectrum. Zn and Al are relatively inexpensive materials, and Al-doped ZnO has emerged as a promising TCO material.[4] $ZnAl_2O_4$ (gahnite) spinel formation has been reported when ZnO is doped with high concentrations of Al.[5] Gahnite is a ceramic with a wide band gap which is transparent for the visible and UV parts of the electromagnetic spectrum.[6] Therefore gahnite might also be seen as a potential economically favorable TCO material. Moreover it is particularly advantageous due to the peculiar arrangement of its cations in the spinel structure. It has been proposed before that such short cation-cation distances lead to a better mobility of the charge carriers.[7]

The materials physics of TCOs can be understood by simple arguments. The basic idea is to create free charge carriers (electrons or holes) in wide-band-gap insulators using either intrinsic defects (e.g., vacancies) or suitable dopants. Defects and impurities in TCOs also play an important role in determining their conductivity. For example, an anion vacancy in a TCO leads to the creation of donor electronic states. If these states are shallow, they contribute additional charge carriers in the conduction band and thereby enhance the conductivity. The cation vacancy, on the other hand, leads to the creation of holes that compensate the extra electrons introduced by means of doping, thereby neutralizing the effect. Also it is observed that undoped as-grown TCO thin films and bulk crystals typically exhibit *n*-type conductivity. The origin of this unintentional conductivity is not clear, and it is often attributed to native point defects.[8] Hence we have undertaken a study of all possible point defects in $ZnAl_2O_4$ in this paper that includes the cation/anion vacancy and antisite defects in which one type of cation is replaced by the other. Note that the antisite defect Al at the Zn site can also be considered as doping $ZnAl_2O_4$ with Al. Al is a shallow donor in ZnO, and here we will study its character in $ZnAl_2O_4$. To the best of our knowledge such a study is not available. Only a limited set of defects in $ZnAl_2O_4$ has been studied by Pandey *et al.*[9] using two-body interatomic potentials. With the recent advances in first-principles calculations based on density functional theory (DFT), a much more accurate understanding of the defect physics can be achieved. Here we present results with the hybrid functional (HSE06) as proposed by Heyd, Scuseria, and Ernzerhof.[10,11] Hybrid functionals correct for the well-known band gap error that is present in DFT when the local-density approximation (LDA) or generalized gradient approximation (GGA) is used. Hybrid functionals have been demonstrated to be a reliable method to calculate transition levels and formation energies of defects.[12]

The results are presented as follows. First, a discussion of the structural properties and the electronic band structure of defect-free $ZnAl_2O_4$ is given. The band alignment of $ZnAl_2O_4$ with wurtzite ZnO is discussed. This is followed by our results on formation energies of various defects in $ZnAl_2O_4$ using a supercell approach. To reflect different experimental growth conditions theoretically, such as Zn rich, O rich, etc., the chemical potential of the constituents is allowed

to vary. This allows a comparison of formation energies of various defects under different growth conditions. The thermodynamic stability of $ZnAl_2O_4$ is discussed in detail. Since charged defects are also possible, transition levels for different charged defects are also reported. Experimentally accessible formation energies under each growth condition are discussed systematically.

II. METHOD AND COMPUTATIONAL DETAILS

Theoretical investigations reported here are based on DFT within the hybrid functional approach, as implemented in the VIENNA AB INITIO SIMULATION PACKAGE (VASP).[13,14] Electron-ion interactions are treated using projector augmented wave (PAW) potentials.[15,16] For the description of spinel Zn ($4s^2 3d^{10}$), Al ($3s^2 3p^1$) and O ($2s^2 2p^4$) are considered valence electrons. A regular $ZnAl_2O_4$ unit cell consists of 14 atoms, viz., 2 Zn, 4 Al, and 8 O atoms. For total energy calculations of defects in the spinel structure, a $2 \times 2 \times 2$ supercell consisting of 112 atoms is considered the starting point. Atoms are removed from their regular lattice site to mimic vacancies while they are removed, and the vacant site is replaced by another type of atom to mimic the antisite defect. Subsequently, the atoms are allowed to relax such that forces on each atomic site are below $\sim$30 meV/Å and simultaneously achieve total energy convergence up to 10^{-4} eV. This convergence is obtained with a Monkhorst-Pack special k-point grid of $2 \times 2 \times 2$. For a faster relaxation of atomic coordinates with the hybrid functional, we have used the GGA optimized coordinates as a starting point.

The defect formation energy $E_f[D^q]$ for a defect D in a charge state q is defined as

$$E_f[D^q] = E_{\text{tot}}[D^q] - E_{\text{tot}}[\text{bulk}] + \sum_i n_i \mu_i + q[E_F + E_v + \Delta V], \quad (1)$$

where $E_{\text{tot}}[D^q]$ is the total energy of the supercell containing the defect, $E_{\text{tot}}[\text{bulk}]$ is the total energy of the supercell without defects, n_i is the number of atoms of type i ($n_i < 0$ if atoms are added, and $n_i > 0$ if atoms are removed), and μ_i is the corresponding chemical potential. E_F is the Fermi energy with respect to the top of the valence band, E_v, of the primitive unit cell. ΔV is the difference in the reference potential of the supercell without defects and the supercell with defects.

Evaluation of the formation energy for different charged defects allows one to find the transition level between two different charged states [$\epsilon(q/q')$]. It is the Fermi energy for which two different charged states have the same formation energy. These transition levels can be observed in experiment with deep-level transient spectroscopy (DLTS). Five charged states, -2, -1, 0, 1, and 2, are considered, and only the transition points for the ones with the lowest formation energy are mentioned in the next section. Additionally, we also consider +3 charged states for Al vacancy and Al_{Zn} antisite defects owing to the three valence electrons of Al.

III. ACCESSIBLE CHEMICAL POTENTIALS

Equation (1) indicates that the defect formation energy depends sensitively on the chemical potential of both atomic species and electrons (often referred to as the Fermi energy E_F). This is because, in forming the defect, particles are exchanged between the host material and the chemical reservoirs. For example, to form the antisite defect Al_{Zn} in $ZnAl_2O_4$ one has to remove a Zn atom from the host and put it into the Zn chemical reservoir, then take an Al atom from the Al chemical reservoir and put it into the host. Therefore, the formation energy of Al_{Zn} decreases if the chemical potential of Al increases. Furthermore, to form a positively charged defect ($q > 0$), one has to put the electrons removed from the defect into an electron reservoir with its characteristic energy E_F. Thus, the positively charged defect will have a higher formation energy in an n-type sample in which the Fermi energy is close to the conduction band minimum (CBM). Similarly, negatively charged defects ($q < 0$) will have a higher energy in p-type material in which the Fermi energy is close to the valence band maximum (VBM). Therefore, by adjusting the chemical potential of the dopant or the Fermi energy, one can control the dopant solubility.

The chemical potential depends on the experimental growth conditions, which can vary from X poor to X rich, where X could be either Zn, Al, or O. We first illustrate the possible variation of the chemical potential for the binary system ZnO and then will extend it to the ternary system $ZnAl_2O_4$. This method follows the formalism proposed by Wei *et al.*[17,18] The formation energy of ZnO is given by

$$\begin{aligned}\Delta H_f^{\text{ZnO}} &= E[\text{ZnO}] - E[\text{Zn}_{\text{bulk}}]/\text{atom} - \tfrac{1}{2}E[\text{O}_2(\text{molecule})] \\ &= E[\text{ZnO}] - \mu_{\text{Zn}}^{\text{Zn bulk}} - \mu_{\text{O}}^{\text{O}_2\text{molecule}} \\ &= \Delta\mu_{\text{Zn}} + \Delta\mu_{\text{O}} \\ &= -3.71 \text{ eV},\end{aligned}$$

where $\Delta\mu_{\text{Zn}} = \mu_{\text{Zn}}^{\text{ZnO}} - \mu_{\text{Zn}}^{\text{Zn bulk}}$ and $\Delta\mu_{\text{O}} = \mu_{\text{O}}^{\text{ZnO}} - \mu_{\text{O}}^{\text{O}_2\text{molecule}}$ (here $\mu_{\text{Zn/O}}^{\text{ZnO}}$ corresponds to the energy of a Zn/O atom in ZnO, $\mu_{\text{Zn}}^{\text{Zn bulk}}$ corresponds to the energy of a Zn atom in bulk Zn, and $\mu_{\text{O}}^{\text{O}_2\text{molecule}}$ corresponds to the energy of an O atom in an oxygen molecule), indicating the possible variation of the Zn and O chemical potential when ZnO is formed. In order to avoid the elemental precipitation into bulk Zn and oxygen gas, respectively, $\Delta\mu_{\text{Zn}}$ and $\Delta\mu_{\text{O}} \leqslant 0$. The upper limit on the Zn chemical potential is set by the Zn-rich conditions: $\mu_{\text{Zn}}^{\text{ZnO}} = \mu_{\text{Zn}}^{\text{Zn bulk}}$ and $\Delta\mu_{\text{Zn}} = 0$. The oxygen chemical potential corresponding to the Zn-rich conditions is then determined as $\Delta\mu_{\text{O}} = \Delta H_f^{\text{ZnO}} = -3.71$ eV. Similarly, the O-rich conditions imply $\mu_{\text{O}}^{\text{ZnO}} = \mu_{\text{O}}^{\text{O}_2\text{molecule}}$ and $\Delta\mu_{\text{O}} = 0$. The zinc chemical potential corresponding to the O-rich conditions is then $\Delta\mu_{\text{Zn}} = \Delta H_f^{\text{ZnO}} = -3.71$ eV.

For ternary systems, the chemical potentials of each constituent species can be varied to reflect specific equilibrium growth conditions but are always globally constrained by the calculated formation enthalpy of the host in order to maintain its stability. Thus in the case of $ZnAl_2O_4$ spinel,

$$\Delta H_f^{\text{ZnAl}_2\text{O}_4} = \Delta\mu_{\text{Zn}} + 2\Delta\mu_{\text{Al}} + 4\Delta\mu_{\text{O}} = -23.21 \text{ eV}. \quad (2)$$

It should be noted that $\Delta\mu_{\text{Zn}} = \mu_{\text{Zn}}^{\text{ZnAl}_2\text{O}_4} - \mu_{\text{Zn}}^{\text{Zn bulk}}$ and $\Delta\mu_{\text{Al}}$, $\Delta\mu_{\text{O}}$ are also defined in a similar way. In addition to the host condition [Eq. (2)], to avoid the elemental precipitation (Zn/Al

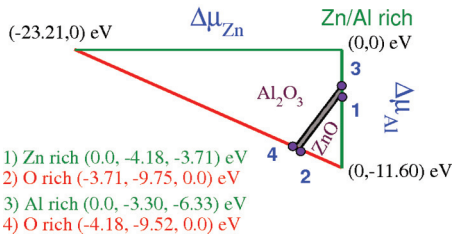

FIG. 1. (Color online) Schematic illustration for the accessible chemical potential range.

solid or oxygen gas) the upper limits are set as

$$\Delta\mu_{\mathrm{Zn}} \leqslant 0, \quad \Delta\mu_{\mathrm{Al}} \leqslant 0, \quad \Delta\mu_{\mathrm{O}} \leqslant 0. \tag{3}$$

The resulting accessible range of the chemical potentials is illustrated in Fig. 1 in a two-dimensional (μ_{Zn}, μ_{Al}) plane. The vertices of the stability triangle are formed from the host condition [Eq. (2)], giving the limits of Zn/Al-rich, Zn-poor, and Al-poor environments, respectively. The Zn-rich condition ($\Delta\mu_{\mathrm{Zn}} = 0$ and $\Delta\mu_{\mathrm{O}} = 0$) leads to the maximum possible variation in the Al chemical potential: $\Delta\mu_{\mathrm{Al}} = \Delta H_f^{\mathrm{ZnAl_2O_4}}/2 = -11.60$ eV. On the other hand, the Al-rich condition ($\Delta\mu_{\mathrm{Al}} = 0$ and $\Delta\mu_{\mathrm{O}} = 0$) leads to $\Delta\mu_{\mathrm{Zn}} = \Delta H_f^{\mathrm{ZnAl_2O_4}} = -23.21$ eV. The line joining the Zn-poor (−23.21, 0.00) and Al-poor (0.00, −11.60) vertices refers to $\Delta\mu_{\mathrm{O}} = 0$ and mimics the oxygen-rich condition. Thus within this triangle the $ZnAl_2O_4$ structure can exist, but the binary structures might have a lower formation energy.

Therefore, the constraints are also imposed by the formation of competing binary oxides ZnO and Al_2O_3, which are

$$\Delta\mu_{\mathrm{Zn}} + \Delta\mu_{\mathrm{O}} \leqslant \Delta H_f^{\mathrm{ZnO}} = -3.71 \text{ eV}, \tag{4}$$

$$2\Delta\mu_{\mathrm{Al}} + 3\Delta\mu_{\mathrm{O}} \leqslant \Delta H_f^{\mathrm{Al_2O_3}} = -19.05 \text{ eV}. \tag{5}$$

These constraints limit the possible accessible range of chemical potentials ($\Delta\mu_{\mathrm{Zn}}$, $\Delta\mu_{\mathrm{Al}}$) for $ZnAl_2O_4$, and the available stable region is shown in gray in Fig. 1. The vertices of this stable region are labeled 1, 2, 3, and 4 and are determined as follows. The first vertex, 1, refers to the Zn-rich condition ($\Delta\mu_{\mathrm{Zn}} = 0$ eV), and using Eq. (4) it leads to $\Delta\mu_{\mathrm{O}} = -3.71$ eV and $\Delta\mu_{\mathrm{Al}} = -4.18$ eV from the stability of the host [Eq. (2)]. The coordinates of the first vertex thus corresponds to $(\Delta\mu_{\mathrm{Zn}}, \Delta\mu_{\mathrm{Al}}, \Delta\mu_{\mathrm{O}}) \equiv (0.00, -4.18, -3.71)$ eV. The second vertex, 2, corresponds to the O-rich condition ($\Delta\mu_{\mathrm{O}} = 0$), resulting in $\Delta\mu_{\mathrm{Zn}} = -3.71$ eV using Eq. (4) and $\Delta\mu_{\mathrm{Al}} = -9.75$ eV from the stability of the host [Eq. (2)]. The coordinates of the second vertex are $(\Delta\mu_{\mathrm{Zn}}, \Delta\mu_{\mathrm{Al}}, \Delta\mu_{\mathrm{O}}) \equiv (-3.71, -9.75, 0.00)$ eV. Below the line joining vertex 1 with vertex 2, Eq. (4) is not fulfilled, and ZnO will form instead of $ZnAl_2O_4$. Similarly, vertices 3 [(0.0, −3.30, −6.33)] and 4 [(−4.18, −9.52, 0.00)] refer to the Al-rich and O-rich conditions, respectively, and are determined from Eq. (5) and from the stability of the host [Eq. (2)]. Above this line, Al_2O_3 will be formed.

For the formation energy plots, we only consider Zn-rich (vertex 1) and O-rich (vertex 2) conditions because the shaded region is rather narrow, indicating the limited accessible range of the chemical potentials. This can be attributed to the fact that the formation enthalpy of $ZnAl_2O_4$ (−1.65 eV/atom) is lower than the stable binary oxides, ZnO (−1.85 eV/atom) and Al_2O_3 (−1.90 eV/atom). Thus, experimentally, it might be difficult to prepare crystalline thin films of $ZnAl_2O_4$.

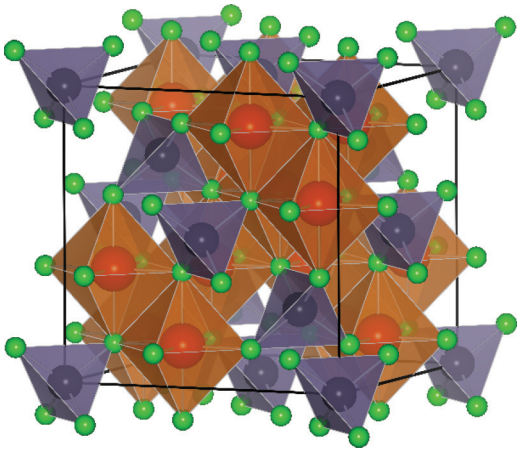

FIG. 2. (Color online) $ZnAl_2O_4$ spinel structure: the Zn atoms in blue are tetrahedrally coordinated with the oxygen atoms shown in green, and the Al atoms (in red) are octahedrally coordinated with the oxygen atoms. The image is generated using VESTA.[19]

IV. RESULTS AND DISCUSSION

1. Structural properties

$ZnAl_2O_4$ adopts the normal spinel structure (space group $Fd\bar{3}m$). It is characterized by the lattice parameter a and an internal parameter u. The Zn atoms are located at Wyckoff position 8a (1/8, 1/8, 1/8) tetrahedral sites, whereas Al atoms are located at the 16d (1/2, 1/2, 1/2) octahedral sites and the O atoms are at 32e (u,u,u) of the fcc structure, as shown in Fig. 2. Both the optimized lattice constant and internal parameter u, calculated using GGA and the HSE06 functional, are in remarkably good agreement with the experiment. These values are reported in Table I.

2. Electronic band structure with HSE06

The electronic band structure of $ZnAl_2O_4$ using standard LDA or GGA has been discussed on several occasions.[21–23] Here, we report the electronic band structure and density of states (DOS) for spinel $ZnAl_2O_4$ calculated using the HSE06 functional (see Fig 3). We have used 37.5% mixing of the Hartree-Fock exchange in the HSE06 functional. This mixing parameter correctly reproduces the experimental value of the band gap in ZnO.[12] $ZnAl_2O_4$ is a direct band gap material with both the VBM and the CBM at Γ. The calculated band

TABLE I. Optimized lattice constant and internal parameter u with the GGA and HSE06 functional.

$ZnAl_2O_4$	GGA	HSE06	Experiment[a]
a (in Å)	8.18	8.06	8.08
u	0.265	0.264	0.263

[a]Reference 20.

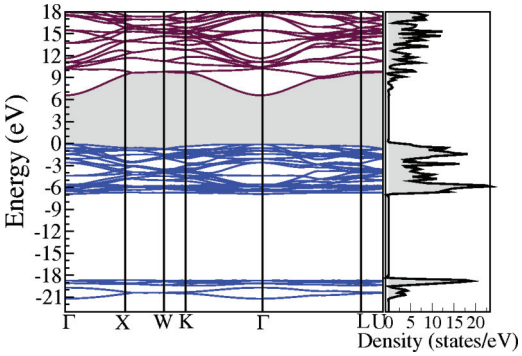

FIG. 3. (Color online) Electronic band structure and density of states calculated using HSE06.

gap with HSE06 is 6.63 eV, which shows a significant opening of the gap compared to the GGA value of 3.83 eV. It also properly accounts for the reported band gap anomaly which is explained in the following. The band gap of $ZnAl_2O_4$ calculated using DFT-LDA is 4.25 eV and is roughly 5% higher than the experimental value of 3.8–3.9 eV. Since DFT typically underestimates the band gap in the oxide system, Sampath *et al.*[23] have claimed that the experimental measurements for $ZnAl_2O_4$ probably require a correction. Using state-of-the-art G_0W_0 calculations, we have supported this claim and expect that the experimental band gap should be around 6.55 eV.[22] The HSE06 band gap is in good agreement with the reported G_0W_0 gap.

3. Band alignment and conductivity

A first indication of the unintentional *n*- and/or *p*-type conductivity of a material can be obtained using a simple branch-point energy (BPE) technique.[24] If the BPE is situated close to the CBM/VBM, the formation of donor/acceptor native defects becomes favorable.[25] One can align the energy bands of different semiconductors using the BPE. The band alignment of wurtzite (wz) ZnO and $ZnAl_2O_4$ spinel is shown in Fig. 4. These are calculated using the HSE06 hybrid functional, which reproduces the experimental band gap of wz ZnO. Comparing with ZnO allows us to estimate the type of unintentional conductivity due to the native point defects in $ZnAl_2O_4$. It is well known that ZnO shows unintentional *n*-type conductivity. $ZnAl_2O_4$ has a larger band gap but with only a small upward shift of the CBM above the CBM of ZnO and is situated above the BPE. The VBM, on the other hand, lies much lower (∼5 eV) than the BPE. Thus from this band alignment result, the formation of a donor defect is favored, and we can clearly exclude the possibility of *p*-type conductivity. Therefore it is also necessary to calculate the formation energy of native defects in $ZnAl_2O_4$ and thereby establish the nature of unintentional conductivity.

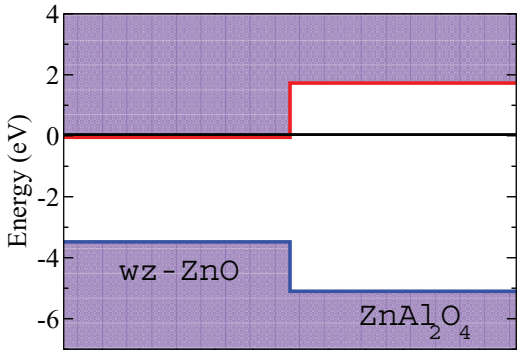

FIG. 4. (Color online) Band alignment in ZnO and $ZnAl_2O_4$. The valence and conduction band edges are represented using blue and red lines, respectively. BPE is used as a reference level and is set to zero.

4. Formation energy with the GGA and hybrid functional

We have studied five point defects in the $ZnAl_2O_4$ lattice: the Al, Zn, and O vacancies along with the antisite defects, Zn replacing Al (Zn_{Al}) and Al replacing Zn (Al_{Zn}). Formation energies of these defects are calculated using the methodology described in the previous section. First, we discuss the formation energies calculated using the GGA (see Fig. 5).

It is expected that the removal of either cation will result in a net electron deficiency and the generation of unoccupied acceptor levels. Such empty defect bands, if situated in or slightly above the VBM, are called shallow acceptors. This results in the production of positive holes (*p*-type carriers) in the valence band, giving rise to *p*-type conductivity. We find

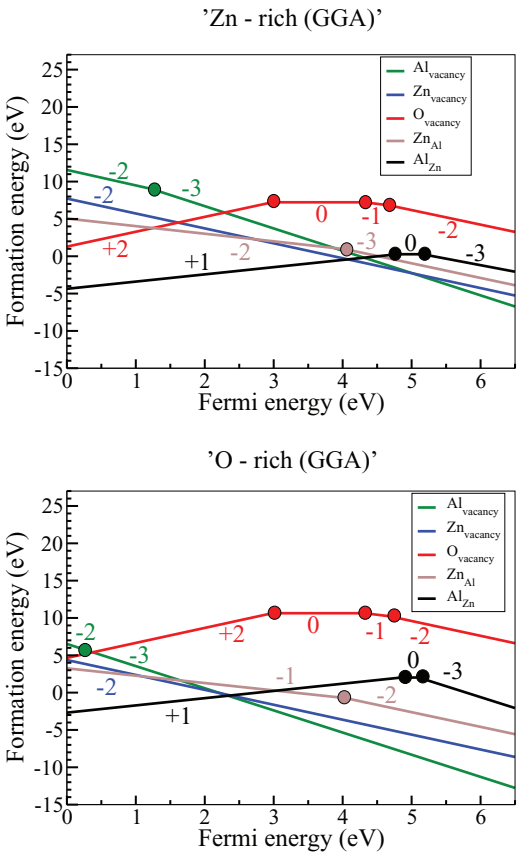

FIG. 5. (Color online) Calculated intrinsic defect formation energies as a function of the Fermi energy under Zn- and O-rich conditions with the GGA. The zero of the Fermi level corresponds to the valence band maximum, and the conduction band minimum is set at the *GW* band gap of 6.55 eV.[22]

that both the Zn and Al vacancies are acceptors and favor the −2 and −3 charge states, respectively. Unfortunately, under Zn-rich (oxygen-poor) conditions, the formation energy of both defects is high, tending toward 8 and 11 eV for the Zn and Al vacancies, as the Fermi level approaches the VBM. A change to oxygen-rich (Zn-poor) conditions reduces the cation chemical potentials, resulting in relatively lower formation energies (about 4 and 7 eV) of the Zn and Al vacancies. However, the formation energies are still large, suggesting that under such conditions, both defects cannot be readily formed.

The oxygen vacancy, on the other hand, exhibits interesting behavior as a function of the Fermi energy. Initially, it favors the +2 charge state, indicating donor-like behavior. The +2/0 transition occurs at about 3.1 eV above the VBM (under Zn-rich conditions), and it continues to prefer the neutral state until ∼4.3 eV, where a 0/−1 transition occurs. Finally, close to the CBM, it becomes an acceptor and prefers the −2 charge state. This suggests that the oxygen vacancy acts as an amphoteric impurity, exhibiting both donor- and acceptor-like behavior depending on the Fermi energy. A similar amphoteric behavior is also shown by the Al_{Zn} antisite defect. However, this is an unexpected result because removal of an anion results in two extra electrons in excess in the system. Similarly, the Al

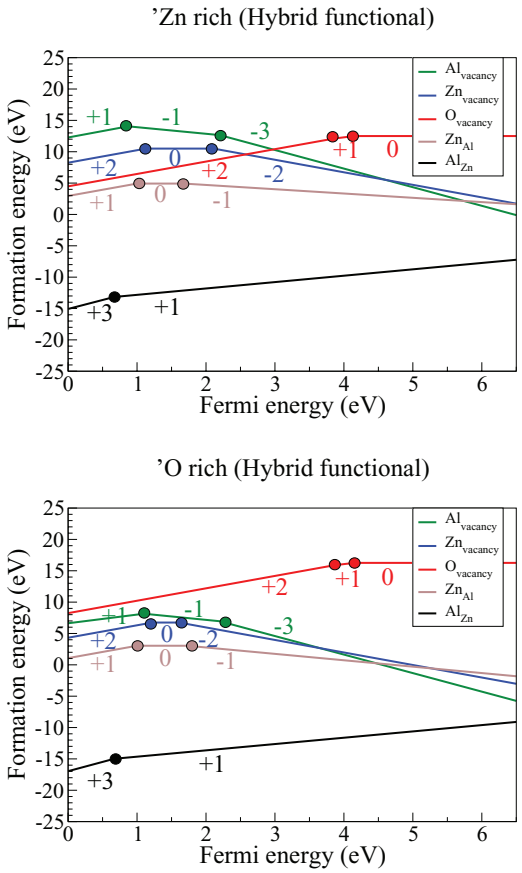

FIG. 6. (Color online) Calculated intrinsic defect formation energies as a function of Fermi energy under Zn- and O-rich conditions with HSE06. The zero of the Fermi level corresponds to the valence band maximum, and the conduction band minimum is set at the GW band gap of 6.55 eV.[22]

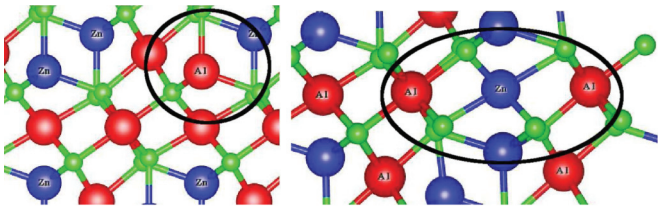

FIG. 7. (Color online) Relaxed atomic geometries for (a) Al_{Zn} and (b) Zn_{Al} antisite defects. The Zn, Al, and O atoms are shown with the blue, red, and green, respectively.

atom contains an extra electron in the valence compared to the Zn atom; the Al_{Zn} antisite defect will also contribute an extra electron in the system. Thus we expect both the oxygen vacancy and the Al_{Zn} antisite defect to prefer a donor state. We believe that it is an artifact due to the strong underestimation of the GGA band gap (3.83 eV) compared to the G_0W_0 value of 6.55 eV. Thus we have calculated the formation energies using the HSE06 functional, which corrects the band gap error and reproduces the G_0W_0 result.

The calculated formation energies as a function of Fermi energy using HSE06 are shown in Fig. 6. The results obtained are different from the previously mentioned GGA calculations. The unexpected amphoteric behavior of the oxygen vacancy and Al_{Zn} antisite defect now disappear. We find that the oxygen vacancy is a really deep donor with the +1/0 transition occurring ∼3 eV below the CBM. It rules out the possibility of oxygen vacancies contributing electrons to the conduction band by thermal ionization. The other two vacancies, namely, the Zn and Al vacancies, are acceptors and prefer the −2 and −3 charged states, respectively. However, their formation energies are high under both metal- and oxygen-rich conditions. Thus these vacancies are also unlikely to contribute the charge carriers at room temperature. The lowest formation energies are observed for the antisite defects: Al_{Zn} and Zn_{Al}. The antisite defect Al_{Zn} initially prefers the +3 charged state, and the +3/ + 1 transition level is situated about ∼0.7 eV above the VBM. Further as a function of the Fermi energy this antisite defect prefers the +1 charged state. Since the +1/0 transition (not shown) occurs just above the CBM, the transition level is a resonance state in the conduction band, and Al_{Zn} acts as a shallow donor. The antisite defect Zn_{Al}, on the other hand, is a deep acceptor.

As discussed, both antisite defects have the lowest formation energy of all native defects. To understand why the formation energy of Al_{Zn} is even lower than Zn_{Al}, it is instructive to analyze further the atomic geometries. Figure 7 shows the relaxed atomic geometries for Al_{Zn} and Zn_{Al} defects. In the spinel structure, the Zn atoms occupy tetrahedral sites, while Al atoms occupy the octahedral positions. When Zn is

TABLE II. Optimized bond lengths for the antisite defect (in Å).

Site	Unrelaxed	Relaxed
Tetrahedral (Al_{Zn})	1.94	1.94
Octahedral (Zn_{Al})	1.90	2.06

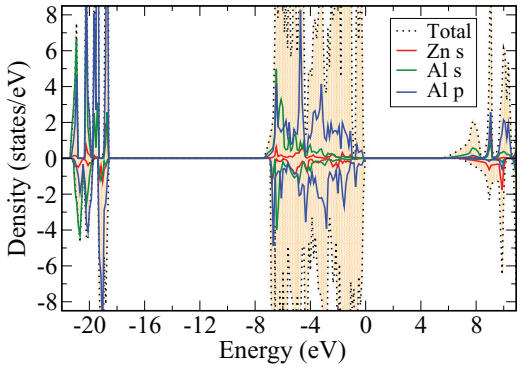

FIG. 8. (Color online) Density of states plot for (top) doped and (bottom) undoped supercells.

replaced by an Al atom, we notice that the cation-anion (Al-O) bond length remains unaltered, as evident in Fig. 7(a). This is because of the smaller atomic radius of the Al atom compared to the Zn atom. On the other hand, when Al is replaced by Zn at the octahedral site, the optimized Zn-O bond length is 2.06 Å, which is ∼8% larger than the Al-O bond. As a consequence, the octahedron is distorted, and oxygen atoms are pushed outward [see Fig. 7(b)] owing to the larger atomic radius of the Zn atom. However, the distance between the second-nearest neighbor is unaffected. The optimized bond lengths are summarized in Table II. Since the bond length remains unaltered for the Al_{Zn} antisite defect, it is energetically more favorable compared to the Zn_{Al} substitution. The facts that (i) the Al_{Zn} antisite defect is a shallow donor and (ii) it is never compensated by the acceptor Zn_{Al} antisite defect lead to our conclusion that $ZnAl_2O_4$ spinel is an intrinsic n-type material.

To find out how the Al_{Zn} antisite defect affects the electronic structure, we now probe the DOS plot for the doped and undoped supercells, as shown in Fig. 8. For undoped $ZnAl_2O_4$, an important contribution to the CBM comes from the Zn s electrons. When Zn is replaced by Al, clearly Al s and Al p peaks appear slightly above the CBM. Thus the DOS plot nicely corroborates with the formation energy calculations as the extra $(3p)$ electron from Al appears in the conduction band, from where it will fall to the CBM. In this way it forms an extended or effective masslike state that can contribute to charge transport.

Figure 9 shows the isosurface of the electron density for undoped and doped supercells containing an Al_{Zn} antisite defect (highlighted by the black ellipse). It can be seen that a large portion of the electron density resides around the oxygen atoms. The Zn-O bond is partially ionic, while the Al-O bond appears even more ionic owing to the transfer of the electron density toward the oxygen. The tetrahedral coordination of the Zn atom and octahedral coordination of the Al atom are also clearly visible in this plot. We observe that in the case of the Al_{Zn} antisite defect, the charge density is localized around the oxygen atom, and this confirms that the antisite defect is ionized. From the DOS and the isosurface plot we can see that when Zn is replaced by Al in the supercell, the impurity-induced state lies in the conduction

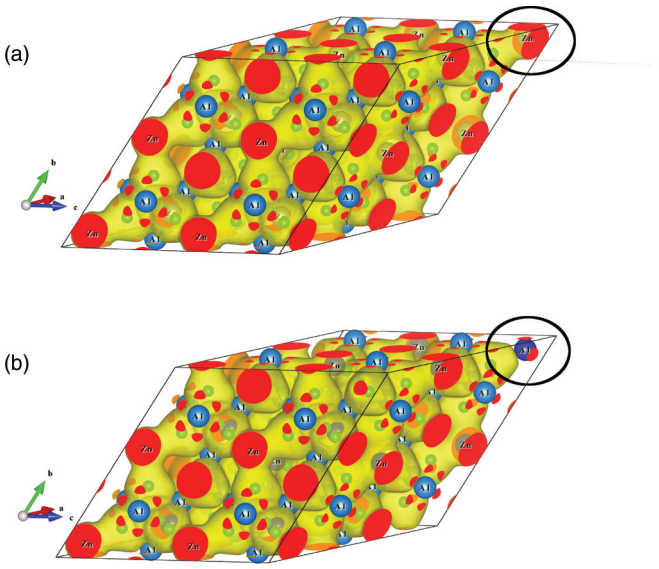

FIG. 9. (Color online) Calculated isosurface of the electron density for (a) undoped and (b) doped (Al_{Zn} antisite defect) supercells. The electron density of the isosurface corresponds to the value of 0.025 e/Å^3. The isosurface sections are shown in red, while the Zn, Al, and O atoms are shown in black, blue, and green, respectively.

band, and the extra $(3p)$ electron is transferred toward the oxygen.

V. CONCLUSIONS

A comparative study of formation energies of native defects in $ZnAl_2O_4$ spinel with GGA and HSE06 clearly shows that the GGA band gap error leads not only to inaccurate defect formation energies but also to wrong conclusions regarding the shallow or deep character of impurities. The hybrid functional corrects the band gap error and hence is essential for an accurate calculation of the formation energy of native defects. The hybrid results indicate that the Al and Zn vacancies are acceptors; however, their formation energies are high. The oxygen vacancy is a deep donor and cannot contribute to the conductivity. The antisite defects have lower formation energies and are the leading cause of disorder in the spinel structure. Among two possible antisite defects, Al_{Zn} has the lowest formation energy under both Zn- and O-rich conditions, and it acts like a shallow donor. The electronic structure shows that the impurity-induced state lies in the conduction band. These results suggest that the Al_{Zn} antisite defect can cause possible n-type conductivity in the $ZnAl_2O_4$ spinel, which corroborates the claim that this material could be a TCO.

ACKNOWLEDGMENTS

We gratefully acknowledge financial support from the IWT-Vlaanderen through the ISIMADE project and the FWO-Vlaanderen through Projects No. G.0191.08 and No. G.0150.13. This work was carried out using the HPC infrastructure of the University of Antwerp (CalcUA), a division of the Flemish Supercomputer Center (VSC), which is funded by the Hercules foundation and the Flemish government (EWI department).

*Present address: Department of Physics, Worcester Polytechnic Institute, Worcester, Massachusetts 01609, USA.

[1]M. Chen, Z. L. Pei, C. Sun, J. Gong, R. F. Huang, and L. S. Wen, Mater. Sci. Eng. B **85**, 212 (2001).
[2]P. Gorm, M. Sander, J. Meyer, M. Kroger, E. Becker, H. H. Johannes, W. Kowalsky, and T. Riedl, Adv. Mater. **18**, 738 (2006).
[3]K. Schulze, B. Maennig, K. Leo, Y. Tomita, C. May, J. Hopkes, E. Brier, E. Reinold, and P. Bauerle, Appl. Phys. Lett. **91**, 073521 (2007).
[4]H. Agura, A. Suzuki, T. Matsushita, T. Aoki, and M. Okuda, Thin Solid Films **445**, 263 (2003).
[5]J. Wiff, Y. Kinemuchi, H. Kaga, C. Ito, and K. Watari, J. Eur. Ceram. Soc. **29**, 1413 (2009).
[6]F. L. L. Zou, X. Xiang, D. G. Evans, and X. Duan, Chem. Mater. **18**, 5852 (2006).
[7]H. Kawazoe and K. Ueda, J. Am. Ceram. Soc. **82**, 3330 (1999).
[8]A. Janotti and C. G. Van de Walle, Phys. Rev. B **76**, 165202 (2007).
[9]R. Pandey, J. D. Gale, S. K. Sampath, and J. M. Recio, J. Am. Ceram. Soc. **82**, 3337 (1999).
[10]J. Heyd, G. E. Scuseria, and M. Ernzerhof, J. Chem. Phys. **118**, 8207 (2003).
[11]J. Heyd, J. Peralta, G. E. Scuseria, and R. L. Martin, J. Chem. Phys. **123**, 174101 (2006).
[12]A. Janotti and C. G. Van de Walle, Phys. Status Solidi. B **248**, 799 (2011).
[13]G. Kresse and J. Furthmüller, Comput. Mater. Sci. **6**, 15 (1996).
[14]G. Kresse and J. Furthmüller, Phys. Rev. B **54**, 11169 (1996).
[15]G. Kresse and D. Joubert, Phys. Rev. B **59**, 1758 (1999).
[16]P. E. Blöchl, Phys. Rev. B **50**, 17953 (1994).
[17]S.-H. Wei, Comput. Mater. Sci. **30**, 337 (2004).
[18]A. Walsh, Y. Yan, M. M. Al-Jassim, and S.-H. Wei, J. Phys. Chem. C **112**, 12044 (2008).
[19]K. Momma and F. Izumi, J. Appl. Crystallogr. **44**, 1272 (2011).
[20]R. Hill, J. R. Graig, and G. Gibbs, Phys. Chem. Miner. **4**, 317 (1979).
[21]S. López, A. H. Romero, P. Rodríguez-Hernández, and A. Muñoz, Phys. Rev. B **79**, 214103 (2009).
[22]H. Dixit, N. Tandon, S. Cottenier, R. Saniz, D. Lamoen, B. Partoens, V. Van Speybroeck, and M. Waroquier, New J. Phys. **13**, 063002 (2011).
[23]S. K. Sampath, D. G. Kanhere, and R. Pandey, J. Phys. Condens. Matter **11**, 3635 (1999).
[24]A. Schleife, F. Fuchs, C. Rödl, J. Furthmüller, and F. Bechstedt, Appl. Phys. Lett. **94**, 012104 (2009).
[25]P. D. C. King, T. D. Veal, P. H. Jefferson, S. A. Hatfield, L. F. J. Piper, C. F. McConville, F. Fuchs, J. Furthmüller, F. Bechstedt, H. Lu, and W. J. Schaff, Phys. Rev. B **77**, 045316 (2008).